Optimizing the electroforming process to enhance the thickness uniformity of full shell X-ray optics

Panini Singam[a], Chet Speegle[b], Amy Meekham[c], Jeffery Kolodziejczak[b], Wayne Baumgartner[b], Grant Davis[d], David Banks[c], Jessica Gaskin[b], Stephen Bongiorno[b], and Brian Ramsey[b]

[a]NASA Post Doctoral Fellow, Oak Ridge Associated Universities, Oak Ridge, Tn.37830, USA
[b]NASA Marshall Space Flight Center, Huntsville, Al, 35805, USA
[c]Jacobs Engineering Group inc., Tullahoma, TN, 37388, USA
[d]University of Alabama in Huntsville, AL, 35805, USA

ABSTRACT

Electroforming replication technology at Marshall Space Flight Center has a long heritage of producing high-quality full-shell X-ray mirrors for various applications. Nickel alloys are electroformed onto a super-polished mandrel in the electroforming process, then separated to form the replicated full-shell optic. Various parameters in the electroplating configuration could result in the nonuniformity of the shell's thickness. Thickness non-uniformities primarily occur due to non-uniform electric field distributions in the electroforming tank during the deposition. Using COMSOL Multiphysics simulations, we have studied the electric field distributions during the deposition process. Using these studies, we have optimized the electric fields inside the tank using customized shields and insulating gaskets on the mandrel. These efforts reduced thickness non-uniformity from over 20% to under 5% percent. Improving the thickness uniformity of the shell aids in better mounting and alignment of shells in the optics module. Optimization of the electroforming process, in some cases, improved the optical performance of the shells. COMSOL optimizing of the electroforming process and the experimental results validating these simulations are presented in this article.

Keywords: X-ray optics, Electroforming, Astrophysics, High-resolution imaging, COMSOL simulations

1. INTRODUCTION

Electroformed replicated technology is a proven technique for fabricating astronomical X-ray optics. The ability to produce full shell, lightweight, and reliable high-resolution optics has made this technology attractive for developing high-throughput astronomical X-ray telescopes. NASA Marshall Space Flight Center (MSFC) has three decades of experience developing grazing incidence X-ray optics through electroformed replication.[1,2,3] In this approach, electroless-Nickel-coated aluminum mandrels are super-polished to match the desired optics prescription and the required surface roughness. After placing it in the electroforming tank and growing the desired thickness Nickel alloy shell, it is carefully separated by cooling the mandrel. We currently use a Nickel Cobalt (NiCo) alloy for electroforming due to its high tensile strength and Young's modulus. The inner surface of the replicated NiCo shell is an exact replica of the polished mandrel surface profile and roughness. A single mandrel can be reused to replicate multiple shells without significantly degrading the surface quality, making it a cost-effective technique for producing many mirror shells.

As the total external reflection of X-rays is limited to small graze angles (typically < 1), the effective geometric area of the optic is scaled down by a factor of the sine of the grazing angle. To increase the effective area, multiple confocal shells with different diameters and graze angles are arranged concentric to each other. The thickness of each shell limits this arrangement. The electroforming replication process produces thin, full shells that are easier to align and mount than segmented-type mirrors. Once the mandrels are polished, replication is relatively inexpensive, making multiple identical mirror modules on a single observatory beneficial. XMM-Newton[4] and

Further author information: (Send correspondence to Panini Singam)
E-mail: srikanthpanini.singam@nasa.gov

IXPE[5] are two examples of this. Pioneering replication technology over the last couple of decades, MSFC has produced X-ray optics for balloon flights (HERO[6,7]), rocket flights (FOXSI-I,[8] FOXSI-II,[9] FOXSI-III[10]) and orbiting satellites (ART-XC,[11] IXPE[5]). Replication technology has also made high-resolution X-ray/Neutron imaging optics for the National Ignition Facility (NIF)[12] and Neutron imaging optics for the National Institute of Standards and Technology (NIST).

While replication produces mirrors about two orders of magnitude thinner than those used for the Chandra mirrors,[13] they have yet to achieve sub-arcsecond angular resolution. Residual profile errors from mandrel polishing, electroforming stresses, shell separation stresses, and mounting errors contribute to performance degradation. We continue to investigate improving these processes at various stages of fabrication to meet the angular resolution requirement for the Lynx mission concept.[14] Ensuring shell thickness uniformity is vital for producing high-quality optics and optimally aligning and mounting shells into mirror module assemblies. Optimization of the electroforming process, in some cases, even improves the optical performance of the shells. Using COMSOL simulations and experimental diagnostic tools, we study and optimize the electric field distribution present during mirror shell electro-deposition. An overview of the electroforming process is described in Section 2, and simulation and experimental results are presented in Section 3 and Section 4, respectively.

2. NICKEL-COBALT ELECTROFORMING REPLICATION PROCESS

In the electroforming process, material from the anodes is electrodeposited onto the mandrel, which acts as a cathode. Unlike traditional electroplating, the mandrel surface is passivated with an oxide layer to reduce the adhesion of the plated material. We use Nickel (Ni) and Cobalt (Co) anodes to deposit NiCo alloy on the mandrel. Pure Nickel is a very ductile material showing signs of yielding at low applied stresses. We have observed that the yield strength of NiCo with an 85 to 15 percent ratio of Ni to Co is much higher and produces stable shells.[2] We use Nickel Sulfamate as an electrolyte whose properties are regulated to have optimal deposition stress for electroplating. Adhesion control and deposition stress control are vital for successful electroforming. Low adhesion and compressive deposition stress can lead to premature release of the shell during electroforming with the risk of damaging the mandrel. Conversely, high adhesion and large tensile deposition stress deform the shell making it difficult to release from the mandrel.[15] Deposition stresses are controlled by regulating the electrolyte temperature and additive salts to the Nickel Sulphamate electrolyte. Deposition rates, controlled by the anode current density, are vital in controlling deposition stresses. Figure 1 shows an example of the measured stress as a function of current density in the electroforming tank.

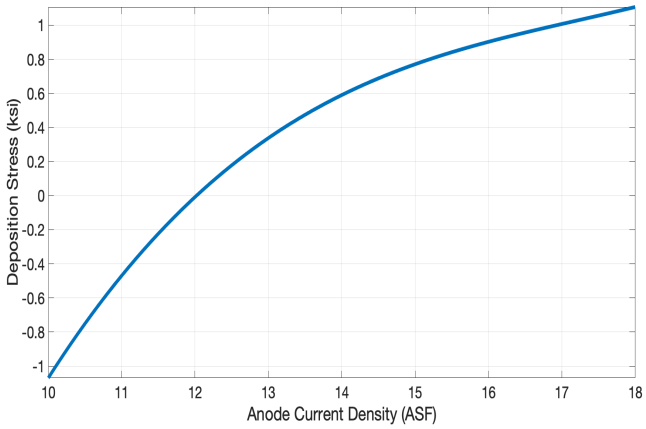

Figure 1: Deposition stress vs. the applied current density of the electroforming tank. Positive deposition stress indicates tensile stress, and negative stress represents compressive stress.

The deposited shell thickness is directly proportional to the local current density on the mandrel surface. The electric field distribution inside the tank depends on the electroforming tank geometry and mandrel dimensions. In the electroforming tank, several anodes are placed symmetrically around the mandrel to ensure azimuthal uniformity of the shell's thickness. The mandrel in the center rotates around its axis throughout the deposition to improve the thickness uniformity. However, due to finite dimensions and the axial slope of the mandrel, the thickness of the shell varies axially. Thickness nonuniformity is more prominent near the shell's ends due to the mandrel surface's abrupt discontinuity. Insulating gaskets and shields regulate the local current densities at the mandrel surface to ensure the uniformity of the axial thickness of the shell. Figure 2 shows the schematic of the electroforming setup with anodes, mandrels, gaskets, and shields.

Our mandrels consist of parabolic and hyperbolic profiles polished onto a monolithic electroless-NiP-coated Aluminium cylinder. Precise polishing at the ends of the mandrels is challenging due to the finite size of the polishing tools. Hence, the axial length of the mandrel on both parabolic and hyperbolic sides is slightly larger than the intended optic dimensions. This end-cap region on either side of the mandrel, which does not form a part of the optic, helps obtain good-quality end regions during polishing. End-cap regions are separated from the optic segment of the mandrels by a small groove (single-piece mandrel) or a detachable block (three-piece mandrel). During the electroforming process, insulating gaskets are used at the boundaries of the optic and end-cap region of the mandrel to restrict plating. Insulating shields are used at both ends of the mandrel to restrict the deposition on the top and bottom sides of the mandrel. Gaskets and shields are primarily used to define the boundaries of the shell. However, their dimensions can be optimized to regulate the local electric field distribution for uniform thickness deposition.

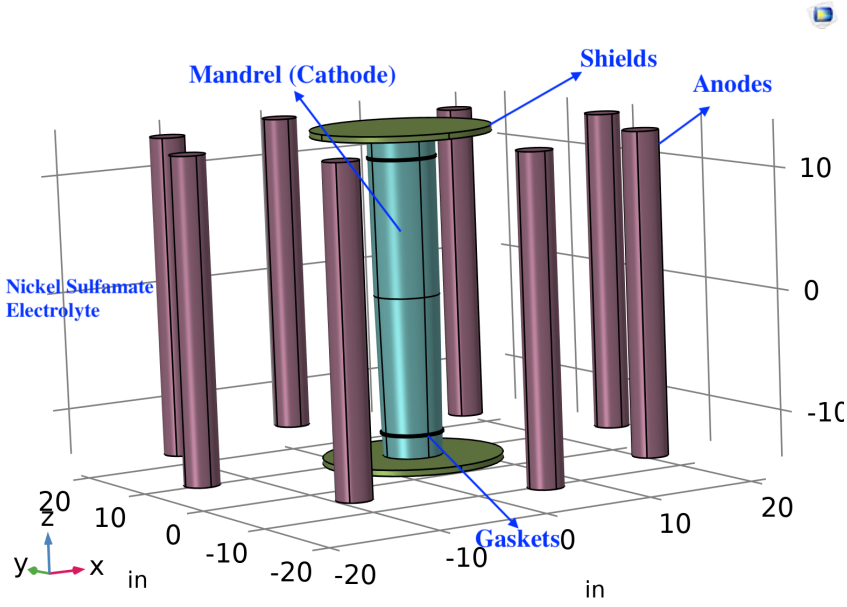

Figure 2: Schematic of the electroforming tank.

3. COMSOL SIMULATIONS TO OPTIMIZE THE ELECTROFORMING PROCESS

We use the COMSOL Multiphysics®software package[16] to model the electric field inside the tank for a given geometry and mandrel. COMSOL allows inputting exact tank geometry specifications to calculate the field distribution. The electric field distribution across the mandrel gives a corresponding distribution of deposition thicknesses. Depending on the size and shape of the mandrels, the electric field varies axially, resulting in a non-uniform thickness distribution. Using these simulations, we design optimal dimensions of gaskets and shields to

control the field distribution. As a result, we have observed a significant improvement in the thickness uniformity of the shells.

3.1 Thickness uniformity at the mirror shell boundaries

The electroformed mandrel experiences higher electric fields near the gaskets, resulting in a greater thickness near the edge of the optics. Thickness uniformity can be improved by increasing the radial height of the gasket (GH) above the surface of the mandrel. For a small gasket height of 5 mm, the mirror shell edges are about 19% thicker than the mid-region of the mirror shell. Figure 3 shows the variation in thickness distribution near the shell edges for different gasket heights. Figure 3 (a) shows the thickness distribution of a cylindrical mirror shell using a gasket with 5 mm height. The edges look significantly thicker than the rest of the optic. Figure 3 (b) shows the thickness distribution for a larger diameter gasket with GH of 4 cm above the mandrel surface. Figure 4 shows the axial shell thickness simulation results for various gasket heights. Thickness uniformity at the edges systematically improves as the gasket height is increased. Increasing the gasket height to 4 cm from 5 mm can reduce axial thickness variation to 3.7 % from 19%.

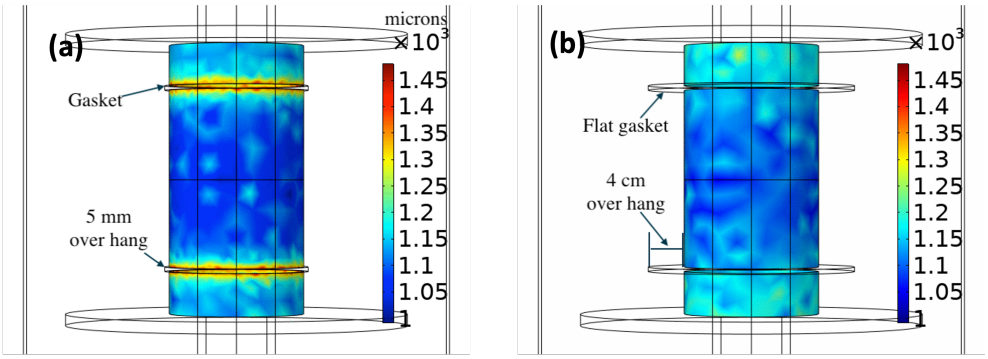

Figure 3: Thickness distribution of mirror shells for gaskets with different heights. (a) the cylinder mandrel with GH= 5 mm. (b) The cylindrical mandrel with GH=4 cm.

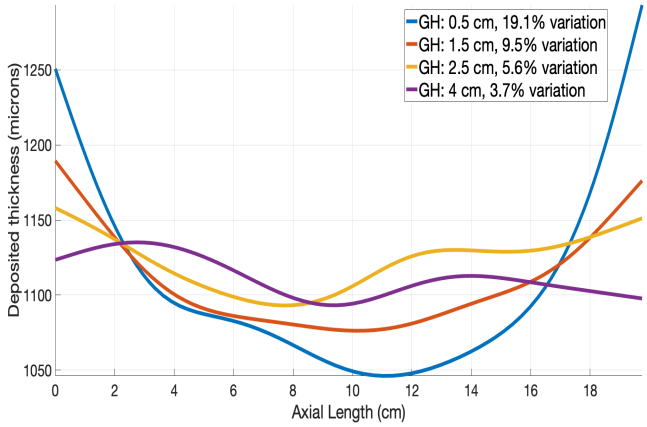

Figure 4: The axial shell thickness simulation results for various gasket heights. The label indicates gasket heights and the corresponding percentage of peak-to-valley thickness variation.

3.2 Gasket optimization for large graze angle optics

As the grazing angle of the optics changes, the relative anode-mandrel distance and slope change. This results in a gradient in the axial thickness of the shell. This effect is more pronounced for the short focal length optics

whose graze angles are noticeably large. The diameters of the mandrel's top and bottom ends are significantly different for large graze angles. Figure 5 shows the axial thickness variation for three different mandrel geometries with varied graze angles. For this simulation, we considered a gasket height of 4 cm to minimize the edge thickness variation. Axial thickness variation increases with the grazing angle of the mandrel. Unlike with small height gaskets, the thickness variation trend is distributed across the axial length of the mandrel. The larger diameter end of the mandrel experiences a higher deposition rate. For a cylindrical mandrel, the axial thickness variation with large gaskets is about 3.7% and looks much flatter across the axial length of the optic. This value significantly increases to 12.3 % for a mandrel with a 3^o graze angle.

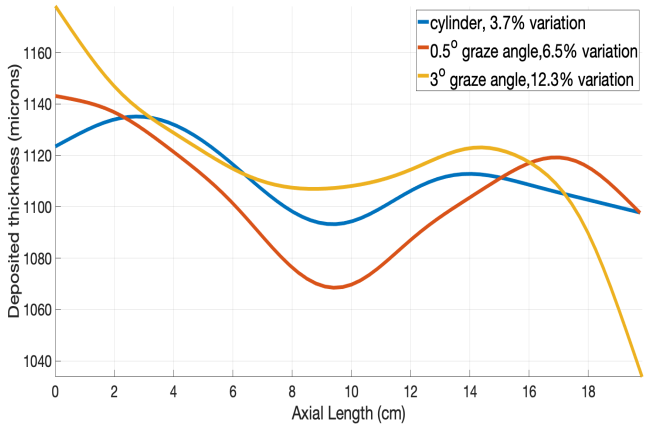

Figure 5: Axial thickness variation for three different mandrels with different graze angles.

The thickness uniformity of the shell with large grazing angles can be improved by using different gasket dimensions for each end of the mandrel. For example, the 3^o graze angle mandrel experiences relatively smaller electric fields on the smaller end of the optic. Optimally reducing the GH on the smaller end increases the electric field to negate this effect. Fixing the GH on the larger end and gradually reducing the GH on the smaller end yields a more uniform thickness distribution. However, if GH is reduced to below the optimal value, the field increases, resulting in much thicker ends. Figure 6 (a) shows the axial thickness distribution for a mandrel with 3^o graze angle for various gasket configurations. The gasket height on the larger end (GH1) is fixed at 4 cm in all cases, while the gasket height on the smaller end (GH2) of the optic is varied for different cases. The optimal configuration with GH2 of 1.5 cm yields about 5.6% thickness variation measured from peak to valley. However, further reducing GH2 to 1 cm above the surface increases the thickness at the smaller end beyond the desired value, resulting in 10.4% variation. Figure 6 (b) shows the schematic of the optimal gasket configuration for a mandrel with a large graze angle.

3.3 Gaskets for single-piece mandrels

Gaskets with large heights, called flat gaskets, are often used with three-piece mandrels. In a three-piece mandrel, the end caps can be detached from the optics portion with the help of screws. Hence, inserting a large flat gasket between the three different parts of the mandrel is easy. However, for a single-piece mandrel, the end caps are part of the primary structure and are separated from the shell-forming region of the mandrel by a machined groove that the gasket sits in. Currently, the groove depth limits the maximum usable GH to 5 mm, resulting in thickness non-uniformity at the edges of the replicated mirror shell.

To maintain the thickness uniformity near the edges of gaskets with smaller GHs, we place a Copper strip around the circumference of the gasket to act as a cathode region. This arrangement redirects the excess electric field from the edges of the forming optics to the gasket. The Copper strip on the gasket gets electroplated, making

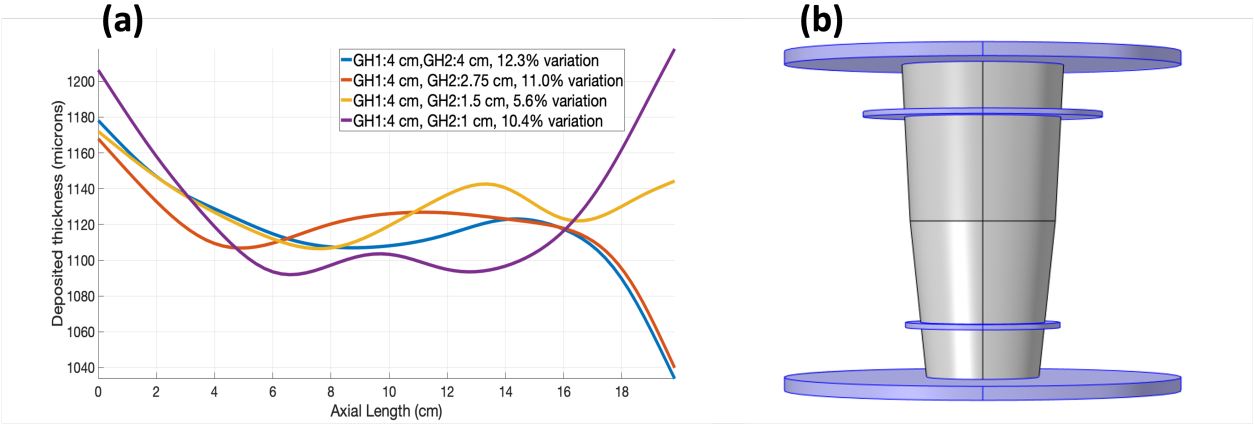

Figure 6: Effect of GH optimization on the axial thickness distribution of the mirror shell. (a) Axial thickness distribution for a mandrel with 3^o graze angle for various gasket configurations. GH1 and GH2 are gasket heights on large and small ends respectively. (b) The schematic of the optimal gasket configuration for a mandrel with a large graze angle. Using different gasket dimensions on each end improves the thickness uniformity.

the optic edges uniform in thickness. Figure 7 shows the effect of the Copper strip on the thickness uniformity of the single-piece mandrel. Figure 7 (a) shows the deposited shell thickness near the gasket without a Copper strip. The optics portion experiences considerable thickness non-uniformity close to the end caps. Figure 7 (b) shows the thickness distribution with a Copper strip on the gasket. The Copper strip gets electroplated, leaving the optics portion with uniform edges. Figure 8 shows the axial thickness variation of the optics with and without the Copper strip on the gasket. Using a Copper strip, thickness uniformity has improved to 7 % from 17 % otherwise.

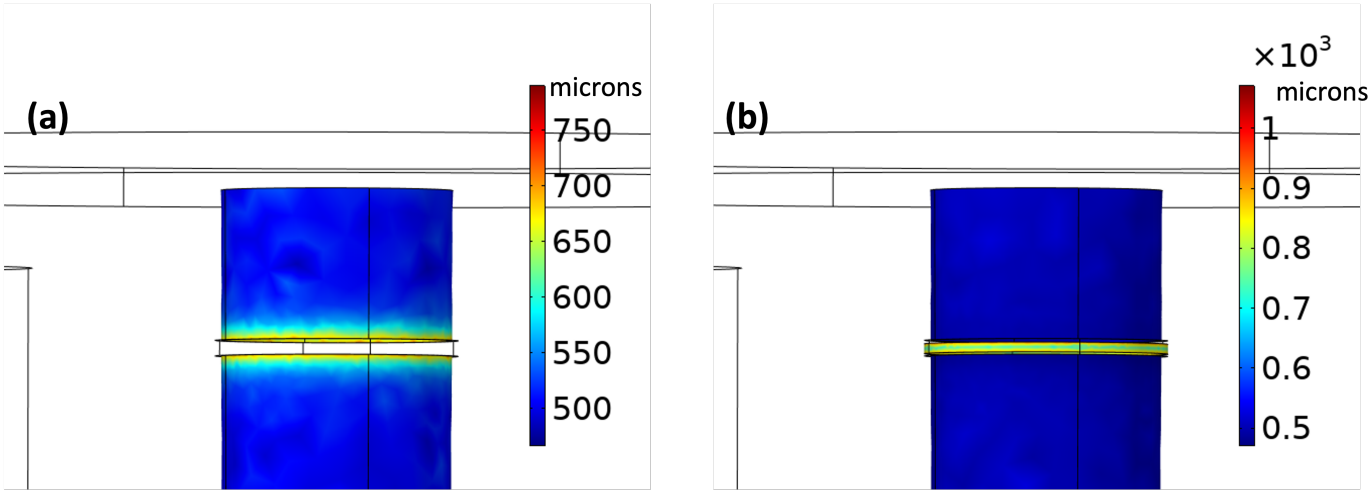

Figure 7: Effect of the gasket Copper strip on the shell thickness uniformity of the single-piece mandrel. The values in the color bar are in microns. (a) Without Cu strip. The optics portion experiences large thickness variation near the end caps. (b) With Cu strip. The Copper strip gets electroplated, leaving the optics portion with uniform edges.

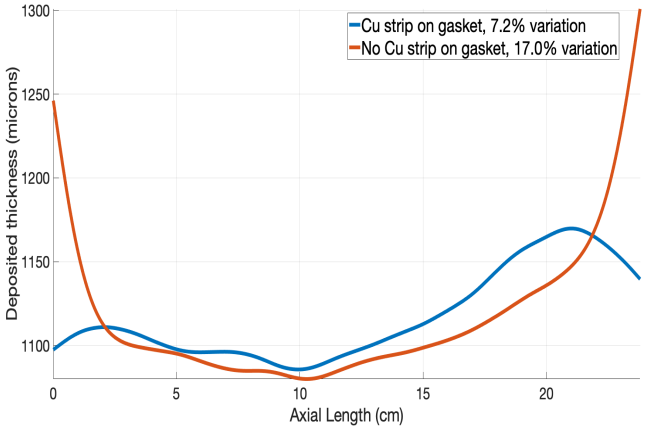

Figure 8: The axial thickness variation of the optics with and without the Copper strip on the gasket. Using a Copper strip, the thickness uniformity has improved to 7 % from 17 %.

3.4 Optimizing shield dimensions for large mandrels

Large diameter gaskets with different GHs on both ends regulates the electric field distribution across the axial surface of the mandrel. However, gaskets of a few centimeters in height cannot influence the total electric field across the surface of a large mandrel. For mandrels with axial lengths larger than about 30 cm, the influence of the gaskets is localized close to the ends. Using extremely large-diameter gaskets of several 10s of centimeters in diameter is impractical and unsafe. Hence we optimize the shield dimensions to regulate the overall electric fields of large mandrels. Even though shields are generally placed at the ends of the mandrel after the end caps, the large shield diameters can influence the field distribution across the mandrel. As the slope on optics makes one end of the mandrel larger than the other, we use different shield diameters on both ends to counter the effect. Figure 9 shows the shell thickness variation of a mandrel with an axial length of 60 cm for various combinations of shield diameters. For this simulation, we have assumed 5 mm diameter gaskets with Copper strips for all the cases. One end of the optics is significantly thicker when using the same diameters for both shields. However, by reducing the shield diameter on one side, the thickness can be increased to closely match the other end. The thickness uniformity is improved to 6.3 % from 8.1 % by changing one of the shields to 56 cm from 76 cm while maintaining the other at 76 cm. Thickness uniformity decreases when the shield diameters are reduced below the optimal value.

4. EXPERIMENTAL VALIDATION OF SIMULATION RESULTS

We have replicated several full-shell X-ray optics based on the inputs from these COMSOL simulations. Optimizing shields and gaskets dimensions has consistently improved the shell thickness uniformity. We replicated a shell from a small three-piece mandrel using large flat gaskets. The mandrel optical axial length is 6.1 cm. The maximum and minimum diameters are 4.6 cm and 4.52 cm, respectively. The mandrel has end caps of 3.9 cm on either side of the optic portion making the total length of the mandrel 13.9 cm. For this three-piece mandrel design, we use flat gaskets having a 2 cm height above the mandrel surface. Figure 10 shows the picture of the mandrel setup with flat gaskets and shields just after plating. After releasing the mirror shell from the mandrel through a cold water bath, we measured the axial thickness using a GE CL5 ultrasonic thickness gauge. The experimental thickness variation is about 2.6 %, which agrees closely with the 2.9 % simulation result. Figure 11 compares the experimental measurement of the axial thickness profile to COMSOL simulation results. The measured thickness variation of 2.6 % is significantly lower than the previously replicated optics with non-optimized gaskets. The "as plated" measured shell thickness results are within 90 % of the simulated COMSOL result values.

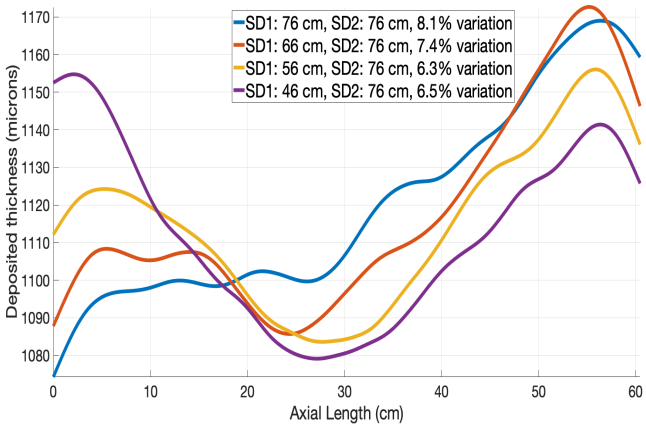

Figure 9: The axial thickness variation of a mandrel with an axial length of 60 cm for various shield diameter combinations.

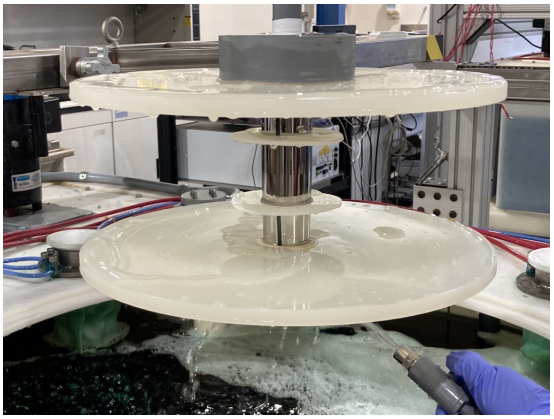

Figure 10: The mandrel setup with flat gaskets and shields just after plating.

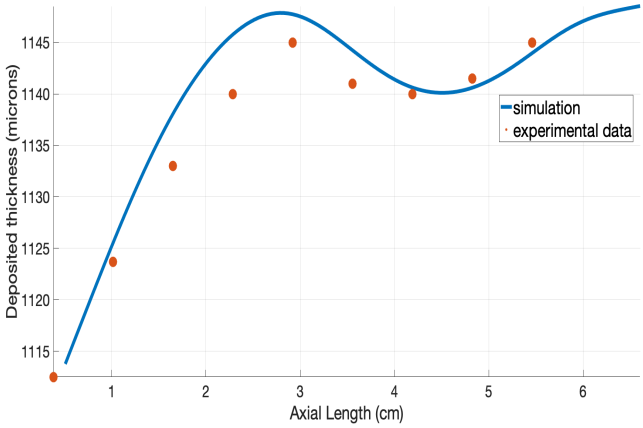

Figure 11: Comparison of the measurement axial thickness profile to the COMSOL simulation results of the configuration shown in figure 10. Thicknesses variation is under 3 % and closely agrees with the simulations.

We have also replicated a shell on a large single-piece mandrel to test the effect of shield optimization. The axial length of the optic is 60 cm. The mandrel has end caps of 5 cm on either side of the optic portion making the total length of the mandrel 70 cm. This optics' maximum and minimum diameters are 7.6 cm and 6.2 cm, respectively. We used a small gasket with a Copper strip to act as a cathode. The shield diameters of the top and bottom ends of the mandrel are 30 cm and 60 cm, respectively. Figure 12 shows the picture of the mandrel with differential shield diameters and Copper strip gaskets used for this experiment. Figure 13 shows the shell's simulated and measured axial thickness after separation. The thickness variation is about 7.5 % and matches closely with the simulation results. Copper cathodes on the gaskets helped to increase the thickness uniformity near the edges of the mirror shell.

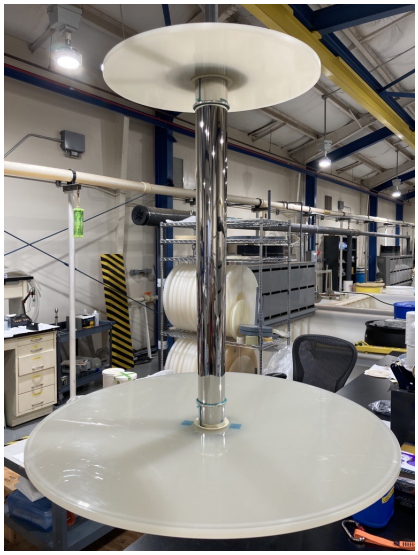

Figure 12: The mandrel with differential shield diameters and Copper strip gaskets.

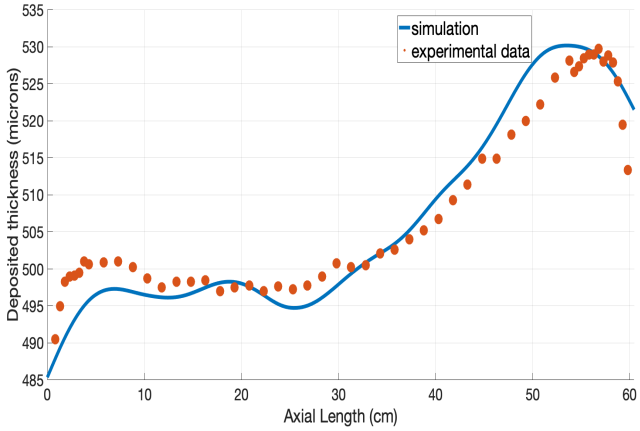

Figure 13: Comparision of the measured axial thickness profile to the COMSOL simulations' predictions for the configuration shown in figure 12. The overall thickness variation is about 7.5 %, as predicted, and closely agrees with the simulation.

5. DISCUSSION AND SUMMARY

Simulations to study the electric field distributions inside the plating tank have proved advantageous in regulating electroformed mirror-shell thickness uniformity. Optimizing gaskets and shield dimensions has consistently produced high-quality optics. Large GHs and Copper strips are used to reduce the edge nonuniformity of the mirror shell, and differential gasket and shield dimensions help to regulate the thickness uniformity across the whole axial length. The thickness distribution in the azimuthal direction is generally uniform due to the rotational symmetry of the tank configuration and mandrel rotation during plating. We repeatedly produce full-shell X-ray optics with under 5 % axial thickness variation using this simulation-led technique. Thickness nonuniformity at the edge of the shell could result in unstable assembly and mounting. As the deposition stress is directly proportional to the local current density, gasket optimization could aid in better shell separation from the mandrel and improved final figures. The optimization process is more critical for optics with large graze angles. We routinely custom-design a unique set of gaskets and shields for each mandrel geometry. In some cases, with small axial length mirrors, using custom gaskets has also improved the imaging performance of the optics. However, we need further investigations to understand this relationship. We are currently investigating the effect of thickness uniformity on the shell release mechanism and non-circularity of the shell.

REFERENCES

[1] Ramsey, B. D., Elsner, R. F., Engelhaupt, D. E., O'Dell, S. L., Speegle, C. O., and Weisskopf, M. C., "Development of hard x-ray optics at MSFC," in [*X-Ray and Gamma-Ray Telescopes and Instruments for Astronomy*], Truemper, J. E. and Tananbaum, H. D., eds., **4851**, 631 – 638, International Society for Optics and Photonics, SPIE (2003).

[2] Ramsey, B., "Replicated Nickel Optics for the Hard-X-Ray Region," *Experimental Astronomy* **20**, 85–92 (2005).

[3] Kilaru, K., Ramsey, B. D., Baumgartner, W. H., Bongiorno, S. D., Broadway, D. M., Champey, P. R., Davis, J. M., O'Dell, S. L., Elsner, R. F., Gaskin, J. A., Johnson, S. A., Kolodziejczak, J. J., Roberts, O. J., Swartz, D. A., and Weisskopf, M. C., "Full-shell x-ray optics development at NASA Marshall Space Flight Center," *Journal of Astronomical Telescopes, Instruments, and Systems* **5**(2), 021010 (2019).

[4] Jansen, F., Lumb, D., Altieri, B., Clavel, J., Ehle, M., Erd, C., Gabriel, C., Guainazzi, M., Gondoin, P., Much, R., Munoz, R., Santos, M., Schartel, N., Texier, D., and Vacanti, G., "Xmm-newton observatory* - i. the spacecraft and operations," *A&A* **365**(1), L1–L6 (2001).

[5] Ramsey, B. D., Attina, P., Baldini, L., Barbanera, M., Baumgartner, W. H., Bellazzini, R., Bladt, J., Bongiorno, S. D., Brez, A., Castellano, S., Carpentiero, R., Castronuovo, M., Cavalli, L., Cavazutti, E., D'Amico, F., Citraro, S., Costa, E., Deininger, W. D., D'Alba, E., Delmonte, E., Dietz, K. L., Lalla, N. D., Marco, A. D., Persio, G. D., Donnarumma, I., Fabiani, S., Ferrazzoli, R., Footdale, J., Head, M., Kalinowski, W., Kolodziejczak, J. J., Latronico, L., Lefevre, C., Lorenzi, P., Lucchesi, L., Maldera, S., Manfreda, A., Mangravati, E., Marshall, H. L., Matt, G., Minuti, M., Mize, R., Muleri, F., Nasimi, H., Negri, B., Nuti, A., O'Dell, S., Orsini, L., Osborne, D., Pentz, C., Pilia, M., Perri, M., Pesce-Rollins, M., Peterson, C., Pinchera, M., Puccetti, S., Rankin, J., Ratheesh, A., Romani, R. W., Sarra, P., Santoli, F., Sciortino, A., Schroeder, C., Sgro, C., Soffitta, P., Spandre, G., Tennant, A., Tobia, A., Thomas, N. E., Trois, A., Vimercati, M., Wedmore, J., Weisskopf, M. C., Xie, F., Zanetti, F., Alexander, C., Allen, D. Z., Amici, F., Andersen, J., Antonelli, A., Antoniak, S., Bachetti, M., Baggett, R. M., Bonino, R., Boree, C., Borotto, F., Breeding, S., Brienza, D., Byggott, H. K., Caporale, C., Cardelli, C., Ceccanti, M., Centrone, M., Dolan, D., Evangelista, Y., Ferrant, K., Ferrie, M., Forsyth, B., Foster, M., Garelick, B., Gunji, S., Gurnee, E., Hibbard, G., Johnson, S., Kelly, E., Kilaru, K., Monaca, F. L., Roy, S. L., Lofredo, P., Maddox, T., Magazzu, G., Marengo, M., Marrocchesi, A., Massaro, F., Mauger, D., McCracken, J., McEachen, M., Mereu, P., Mitchell, S., Mitsuishi, I., Morbidini, A., Mosti, F., Nguyen, T., Negro, M., Nitschke, I., Onizuka, M., Oppedisano, C., Pacheco, R., Paggi, A., Painter, W., Pavelitz, S. D., Piazzolla, R., Profeti, A., Ranganathan, J., Reedy, L., Root, N., Rubini, A., Ruswick, S., Sanchez, J., Scalise, E., Seek, T., Sosdian, K., Speegle, C. O., Tamagawa, T., Tardiola, M., Valerie, R., Walden, A. L., Weddendorf, B., and Welch, D., "The Imaging X-Ray Polarimetry Explorer (IXPE): technical overview IV," in [*UV, X-Ray, and Gamma-Ray Space Instrumentation for Astronomy XXII*], Siegmund, O. H., ed., **11821**, 118210M, International Society for Optics and Photonics, SPIE (2021).

[6] Ramsey, B. D., Alexander, C. D., Apple, J. A., Austin, R. A., Benson, C. M., Dietz, K. L., Elsner, R. F., Engelhaupt, D. E., Kolodziejczak, J. J., O'Dell, S. L., Speegle, C. O., Swartz, D. A., Weisskopf, M. C., and Zirnstein, G., "HERO: high-energy replicated optics for a hard-x-ray balloon payload," in [*X-Ray Optics, Instruments, and Missions IV*], Hoover, R. B. and II, A. B. C. W., eds., **4138**, 147 – 153, International Society for Optics and Photonics, SPIE (2000).

[7] Gaskin, J., Apple, J., Chavis, K. S., Dietz, K., Holt, M., Koehler, H., Lis, T., O'Connor, B., Otero, M. R., Pryor, J., Ramsey, B., Rinehart-Dawson, M., Smith, L., Sobey, A., Wilson-Hodge, C., Christe, S., Cramer, A., Edgerton, M., Rodriguez, M., Shih, A., Gregory, D., Jasper, J., and Bohon, S., "High energy replicated optics to explore the sun: Hard x-ray balloon-borne telescope," in [*2013 IEEE Aerospace Conference*], 1–11 (2013).

[8] Krucker, S., Christe, S. D., Glesener, L., nosuke Ishikawa, S., Ramsey, B. D., Takahashi, T., Watanabe, S., Saito, S., Gubarev, M. V., Kilaru, K., Tajima, H., Tanaka, T., Turin, P., McBride, S., Glaser, D., Fermin, J., White, S. M., and Lin, R. P., "First images from the focusing optics x-ray solar imager," *The Astrophysical Journal Letters* **793** (2014).

[9] Christe, S. D., Glesener, L., Buitrago-Casas, C., nosuke Ishikawa, S., Ramsey, B. D., Gubarev, M. V., Kilaru, K., Kolodziejczak, J. J., Watanabe, S., Takahashi, T., Tajima, H., Turin, P., Shourt, V., Foster, N., and Krucker, S., "Foxsi-2: Upgrades of the focusing optics x-ray solar imager for its second flight," (2016).

[10] Musset, S., Buitrago-Casas, J. C., Glesener, L., Bongiorno, S. D., Courtade, S., Athiray, P. S., Vievering, J. T., nosuke Ishikawa, S., Narukage, N., Furukawa, K., Ryan, D. F., Dalton, G., Turin, Z., Davis, L., Takahashi, T., Watanabe, S., Mitsuishi, I., Hagino, K., Kawate, T., Turin, P., Christe, S. D., Ramsey, B. D., and Krucker, S., "Ghost-ray reduction and early results from the third foxsi sounding rocket flight," in [*Optical Engineering + Applications*], (2019).

[11] Pavlinsky, M., Levin, V., Akimov, V., Krivchenko, A., Rotin, A., Kuznetsova, M., Lapshov, I., Tkachenko, A., Krivonos, R., Semena, N., Buntov, M., Glushenko, A., Arefiev, V., Yaskovich, A., Grebenev, S., Sazonov, S., Lutovinov, A., Molkov, S., Serbinov, D., Kudelin, M., Drozdova, T., Voronkov, S., Sunyaev, R., Churazov, E., Gilfanov, M., Ramsey, B., O'Dell, S. L., Kolodziejczak, J., Zavlin, V., and Swartz, D., "ART-XC / SRG overview," in [*Space Telescopes and Instrumentation 2018: Ultraviolet to Gamma Ray*], den Herder, J.-W. A., Nikzad, S., and Nakazawa, K., eds., *Society of Photo-Optical Instrumentation Engineers (SPIE) Conference Series* **10699**, 106991Y (July 2018).

[12] Champey, P. R., Kolodziejczak, J., Kozioziemski, B., Davis, J., Griffith, C., Kester, T., Kilaru, K., Meekham, A., Menapace, J., Ramsey, B., Roberts, O. J., Sanchez, J., Singam, P., Smith, W. S., Speegle, C., Stahl, M., Suratwala, T., Thomas, N., Young, M., and Vogel, J. K., "Toward the fabrication of a 5-m-resolution Wolter microscope for the National Ignition Facility (invited)," *Review of Scientific Instruments* **93**, 113504 (11 2022).

[13] Weisskopf, M. C., Tananbaum, H. D., Speybroeck, L. P. V., and O'Dell, S. L., "Chandra X-ray Observatory (CXO): overview</title&gt, booktitle = SPIE Proceedings," SPIE (jul 2000).

[14] Gaskin, J. A., Allured, R., Bandler, S. R., Basso, S., Bautz, M. W., Baysinger, M. F., Biskach, M. P., Boswell, T. M., Capizzo, P. D., Chan, K.-W., Civitani, M. M., Cohen, L. M., Cotroneo, V., Davis, J. M., DeRoo, C. T., DiPirro, M. J., Dominguez, A., Fabisinski, L. L., Falcone, A. D., Figueroa-Feliciano, E., Garcia, J. C., Gelmis, K. E., Heilmann, R. K., Hopkins, R. C., Jackson, T., Kilaru, K., Kraft, R. P., Liu, T., McClelland, R. S., McEntaffer, R. L., McCarley, K. S., Mulqueen, J. A., Özel, F., Pareschi, G., Reid, P. B., Riveros, R. E., Rodriguez, M. A., Rowe, J. W., Saha, T. T., Schattenburg, M. L., Schnell, A. R., Schwartz, D. A., Solly, P. M., Suggs, R. M., Sutherlin, S. G., Swartz, D. A., Trolier-McKinstry, S., Tutt, J. H., Vikhlinin, A., Walker, J., Yoon, W., and Zhang, W. W., "Lynx Mission concept status," in [*UV, X-Ray, and Gamma-Ray Space Instrumentation for Astronomy XX*], Siegmund, O. H., ed., **10397**, 103970S, International Society for Optics and Photonics, SPIE (2017).

[15] Engelhaupt, D., Ramsey, B., and Speegle, C., "Electrodeposition of low stress nickel-phosphorus alloys for precision component fabrication," in [*Proc. SPIE 2000*], (2000).

[16] Multiphysics, C., "Introduction to comsol multiphysics®," *COMSOL Multiphysics, Burlington, MA, accessed Feb* **9**, 2018 (1998).